Loto & Babalola, *Cogent Engineering* (2018), 5: 1473002
https://doi.org/10.1080/23311916.2018.1473002

cogent engineering

MATERIALS ENGINEERING | RESEARCH ARTICLE

Analysis of *SiC* grain size variation and NaCl concentration on the corrosion susceptibility of AA1070 aluminium matrix composites

Roland Tolulope Loto[1]* and Phillip Babalola[1]

Received: 06 February 2018
Accepted: 01 May 2018
First Published: 21 May 2018

*Corresponding author: Roland Tolulope Loto, Department of Mechanical Engineering, Covenant University, Ota, Ogun State, Nigeria
E-mail: tolu.loto@gmail.com

Reviewing editor:
Catherine MacKenzie, Taylor and Francis Group, UK; Guglielmo Lomonaco, Università degli Studi di Genova, Italy

Additional information is available at the end of the article

Abstract: Analysis of the impact *SiC* grain size at 10% wt. on the corrosion resistance of AA1070 aluminium matrix composites was studied in Cl^- anion containing dilute H_2SO_4 solution. Studies were performed with potentiodynamic polarization and open circuit potential (OCP) measurement. Optical microscopic studies were performed on the corroded matrix composites. Results show that the corrosion susceptibility of the composites increased proportionately with increase in Cl^- ion concentration. The matrix composites at 3 um and 9 um *SiC* grain size exhibited the lowest corrosion rate values in comparison to the base alloy and composites with larger *SiC* grain sizes. OCP values for the matrix composite at 0 µm *SiC* in the acid solution (0.25 M H_2SO_4/0% and 0.25% NaCl) was the most electronegative due to lower thermodynamic stability than matrix composites with larger *SiC* grain sizes. Optical microscopic studies show that corrosion was mainly localized for all specimens tested due to pitting at low Cl^- ion concentration in comparison to general corrosion for the metal substrate and total destruction of the matrix composite morphology at higher chloride concentration. Results of statistical analysis through ANOVA showed that *SiC* grain sizes are more

ABOUT THE AUTHORS

Roland Tolulope Loto is a professor at the Department of Mechanical Engineering, Covenant University, Ota, Ogun State, Nigeria. He is the principal investigator of the corrosion and materials research cluster. Roland has over 93 research publications including reviews in top international journals and has consistently served as reviewer in respectable journals due to his in-depth knowledge and technical expertise. Roland is a registered member of the Council for the Regulation of Engineering in Nigeria, South African Institute of Mining and Metallurgy and the Corrosion Institute of Southern Africa.

Philip Babalola (PhD) is a lecturer at the Department of Mechanical Engineering, Covenant University, Ota, Ogun State, Nigeria. He specializes in research on composites, renewable energy applications, pipe network analysis with significant publications. He is a registered member the Council for Regulation of Engineering in Nigeria and corporate member of the Nigerian Society of Engineers.

PUBLIC INTEREST STATEMENT

The economic impact and problems resulting from corrosion has drawn strong attention from scientists and engineers worldwide. Corrosion of aluminium alloys in industrial environments is a major concern in chemical processing plants, oil and gas industry, manufacturing and automobile industry, marine operations, boiler and power generation plants due to the considerable cost involved in the replacement of metallic parts in their various applications. The consequence often leads to plant shutdowns, breakdown of industrial equipment, reduced efficiency, industrial downtime, high maintenance cost due to replacement of damaged part, wastage of valuable resources and expensive overdesign. Corrosion prevention through modification of the metallurgical structure of aluminium with the addition of silicon carbide is of great practical importance and can be extensively employed in curtailing wastage of engineering materials and minimizing costs of corrosion control.

relevant than NaCl concentration in evaluation of the corrosion susceptibility of the matrix composite.

Subjects: Chemistry; Material Science; Materials Science

Keywords: corrosion; silicon carbide; aluminium; sodium chloride; composite

1. Introduction

Corrosion resistance of aluminium alloys is the product of interfacial oxide evolution; however, the oxide is subject to localized breakdown resulting in pitting and general and crevice corrosion of the substrate metal. The major limitation in the application of aluminium alloys for high-performance tribological application in extreme environments is their poor wear properties for engineering applications such as low hardness, poor degradation resistance and weldability, thus the need to develop more efficient materials with greater efficiency without reducing the strength to weight ratio (Sinclair & Gregson, 1997). Aluminium silicon matrix composites (Al-*SiC*) are new generation of engineering materials for applications such as in automobiles, aeronautics, electronics, recreation and military industries (Chawla, 2013; Lees, Dhihra, & McCullough, 2005; Surappa, 2003). They consist of *SiC* grains scattered within aluminium alloy substrate. The desired mechanical properties of aluminium and silicon are admixed to give matrix composites with superior strength, higher specific modulus, enhanced rigidity, lighter weight, lower coefficient of thermal expansion, higher thermal conductivity, customized electrical properties, superior abrasion and damping properties than their unreinforced counterparts (Mahendra, Arulshri, & Iyandurai, 2013; Neelima, Mahesh, & Selvaraj, 2011; Singh & Singla, 2012; Singla, Dwivedi, Singh, & Chawla, 2009). Matrix composites are basically an admixture of contrasting metals and intermetallic compounds ingrained within the substrate metal. The characteristics of the composites is subject to the individual characteristics of the intermetallic phases, their corresponding volume, grain dimension and orientation within the matrix (George, Totten, & Scott, 2003; William, 2007). They transmit applied loads to scattered reinforcements secured with the matrix (Pai, Rajan, & Pillai, 2004). Silicon carbide (*SiC*) is a chemical combination of silicon and carbon elements. It possesses excellent resistance to acids, alkalis and liquefied NaCl till 800°C. It forms a chemically resistant silicon oxide film in air at 1,200°C, with appreciable applicability till 1,600°C. Dispersion of *SiC* substituents within the matrix material is dependent on properties such as deformation and flow of the molten matrix, technique of grain incorporation and their interaction during the admixture process (Hashim, Looney, & Hashmi, 2002).

The major drawback of Al-*SiC* is the extent to which the intermetallic constituents affect the resistance of the aluminium matrix to interfacial degradation. Addition of *SiC* can result in the presence of discontinuities, inclusions and defects in the protective film exposing more areas to corrosion (Trowsdale et al., 1996). The resulting microstructural heterogeneity increases the corrosion susceptibility of Al-*SiC* due to galvanic effect and interfacial issues. Their excellent heat conduction and small expansion coefficients have resulted in applications which expose them to astringent conditions (Bakkar & Neubert, 2007; Candan & Biligic, 2004; Griffiths & Turnbull, 1994). Processing specifications also significantly affect the composite microstructure and, consequently, their corrosion behaviour. Previous research on modification of *SiC* content on aluminium matrix composite in H_2SO_4 solution showed that the presence of *SiC* at low chloride concentration exposed the matrix material to greater corrosion attack (Loto & Babalola, 2017). Result also showed that *SiC* at the lowest content of 10% had the highest corrosion resistance in acid chloride solution. This investigation focuses on the effect of *SiC* grain size variation with respect to chloride concentration on the corrosion susceptibility of AA1070 aluminium. The mechanical properties of aluminium alloys infused with nonmetallic particulates are influenced by the grain size and the volume fraction. Due to lack of improvement in strength and porosity of Al-*SiC*, when the volume fraction of silicon carbide exceeds 10%, this research is limited to 10% silicon carbide content added in the aluminium alloy as reinforcement.

2. Experimental methods

2.1. Materials and preparation

AA1070 aluminium metal (AA1070) was purchased from Aluminium Rolling Mills, Ota, Ogun State, Nigeria. Energy-dispersive spectrometer analysis at Materials Characterization Laboratory, Department of Mechanical Engineering, Covenant University, Ota, Ogun State, Nigeria, gave ostensible (wt.%) constitution shown in Table 1. Silicon carbide (*SiC*) with ostensible (wt.%) constitution shown in Table 2 and of 320 grit size was sourced from Logitech, UK, and added to AA1070 at weight percentages of 10%. A tilting furnace of 20 kg capacity was used to melt AA1070 for 45 min at 650°C. *SiC* was added to molten AA1070, stirred, shaped into moulds (AA1070/*SiC*) and cooled for 24 h. AA1070/*SiC* was sectioned mechanically and metallographically prepared using silicon carbide grinding papers (80, 320, 600, 800 and 1,000 grit) and cleansed with deionized H_2O and propanone for electrochemical tests. Analar grade sodium chloride purchase from Titan Biotech, India, was produced in proportional volumes of 0%, 0.25%, 0.5%, 0.75% and 1% in 200 mL of 0.25 M H_2SO_4 solution, prepared from standard grade of H_2SO_4 acid (98%) with deionized H_2O. Microhardness test, tensile test and electrical conductivity and resistivity tests were performed on AA1070/*SiC* specimens as shown in Table 3. Microhardness test of AA1070/*SiC* specimens were performed with LECO 700AT microhardness tester with a load of 492.3mN and a waiting time of 10 s (ASTM Standard E 384). Six tests were performed for every specimen and the mean value was used as the microhardness value. Instron (Model 3369) Universal Testing Machine with 30 kN load (ASTM International E8/E8M-09) was used to perform tensile test on AA1070/*SiC* specimens. The test specimens with mean cross-sectional dimensions of 5 mm by 10 mm and gauge length of 25 mm were produced and tested five successive times with the measurement taken (modulus) for each sample and the mean value was used as the parameter value. Electrical conductivity and resistivity test was performed on AA1070/*SiC* specimen with Keithley Instruments Model 2400.

Table 1. Percentage constitution of AA1070

Element symbol	Fe	Si	Mn	Cu	Zn	Ti	Mg	Pb	Sn	Al
% constitution	0.232	0.078	0.000	0.0006	0.0016	0.006	0.0027	0.0012	0.007	99.66

Table 2. Percentage constitution of *SiC*

Element symbol	C	Al	Fe	Si	SiO_2	Magnetic Fe	*SiC*
% constitution	0.50	0.30	0.20	0.80	0.0016	0.04	97.6

Table 3. AA1070/*SiC* test results on modulus of elasticity, hardness values and electrical conductivity

S/N	*SiC* grain size (μm) of AA1070/*SiC* samples	Modulus (N/mm^2)	Hardness (HV)	Electrical Conductivity (MV/m)
1	0	402.413	19.6	70.254
2	3	645.463	35.2	50.271
3	9	990.415	34.3	56.635
4	29	760.357	26.2	48.963
5	45	760.357	26.2	48.963

Each specimen with cross-sectional area of 10 mm by 10 mm with length of 100 mm were prepared for testing in 4-point probe set up machine. The working voltage is 20 mV. Voltage, current, resistivity and conductivity were obtained from this setup.

Polarization tests were conducted 37°C with a triple electrode consisting of platinum counter electrodes, Ag/AgCl reference electrodes and embedded AA1070/*SiC* working electrode with visible surface area of 1 cm^2 with a transparent/aerated cell accommodating 200 mL of the test electrolyte media and connected to Digi-Ivy 2311 potentiostat. Anodic/cathodic potentiodynamic polarization curves were produced at 0.0015V/s scan rate between set potentials of −1.25V and +1.5V. Corrosion current density (j_c) and corrosion potential (E_c) values were determined using the Tafel extrapolation method. The corrosion rate (C_R) and the inhibition efficiency (η, %) were calculated from the formulae below:

$$C_R = \frac{0.00327 \times J_c \times E_q}{D} \tag{1}$$

j_c is the current density (A/cm^2), D is the density in (g/cm^3); E_q is the equivalent weight (g) and 0.00327 is the corrosion rate constant (mm/y). Open circuit potential (OCP) values were acquired at 0.05 V/s step potential for 1,500 s. Optical images of AA1070/*SiC* morphology was studied after corrosion with Omax trinocular metallurgical microscope using ToupCam analytical software.

The statistical importance of *SiC* grain size and chloride concentration on the corrosion rate of AA1070/*SiC* was studied through analysis of variance (ANOVA) at 95% confidence (significance level, α = 0.05) with respect to the following equations.

The sum of squares among columns (NaCl concentration)

$$SS_c = \frac{\sum T_c^2}{nr} - \frac{T^2}{N} \tag{2}$$

Sum of squares among rows (*SiC* grain size)

$$SS_r = \frac{\sum T_r^2}{nc} - \frac{T^2}{N} \tag{3}$$

Total sum of squares

$$SS_{Total} = \sum x^2 - \frac{T^2}{N} \tag{4}$$

3. Result and discussion

3.1. Potentiodynamic polarization studies

Anodic–cathodic polarization plots for AA1070/*SiC* with specific *SiC* grain size (3μm, 9 μm, 29 μm and 45 μm *SiC* grain size) in 0.25M H_2SO_4 solution at 0%, 0.25%, 0.5%, 0.75% and 1% NaCl concentration are shown from Figure 1(a) to 1(e). Results of corrosion rate, corrosion potential, corrosion current density, anodic and cathodic Tafel constants and polarization resistance obtained from the polarization test are shown in Table 4. Observation of AA1070 corrosion at 0 μm *SiC* grain size in 0.25M H_2SO_4/0%, 0.25%, 0.5%, 0.75% and 1% NaCl solution shows a relative increase in corrosion rate of AA1070 with increase in Cl^- concentration from 1.185 mm/y at 0% NaCl to 2.251 mm/y at 1% NaCl. AA1070 generally exhibits good corrosion resistance in astringent conditions due to the evolution of a protective oxide on the metal surface. However, Cl^- ions tend to cause instability and possible degradation of the passive film, leading to breakdown and pitting corrosion of the metal. The experiment was conducted in aerated containers; thus it can be concluded that the aluminium metal without *SiC* content was readily polarized in the acid chloride solution. The chlorides probably contributed to the formation of soluble chlorinated aluminium

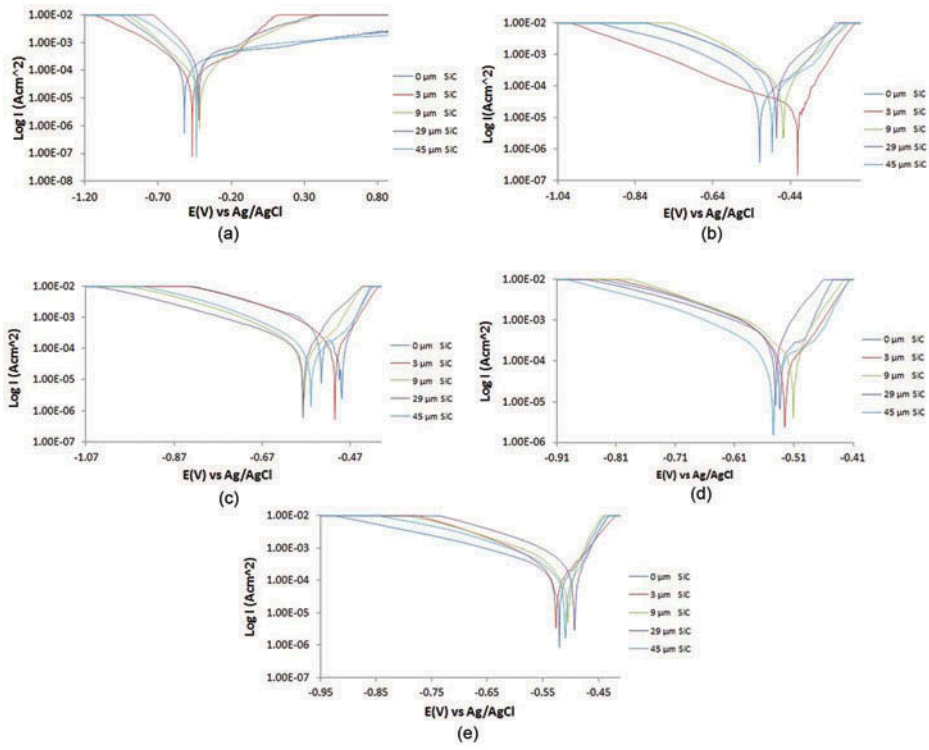

Figure 1. Plot of the anodic–cathodic polarization curves for AA1070/*SiC* (0µm–45 µm) at (a) 0.25M H_2SO_4/0% NaCl, (b) 0.25M H_2SO_4/0.25% NaCl, (c) 0.25M H_2SO_4/0.5% NaCl, (d) 0.25M H_2SO_4/0.75% NaCl and (e) 0.25M H_2SO_4/1% NaCl.

hydroxide in the presence of oxygen, which hindered the formation and or repassivation of the protective oxide.

Addition of 3 µm and 9 µm *SiC* grain size to AA1070 matrix at 0% NaCl concentration improved the corrosion resistance of AA1070/*SiC* with relative reduction in corrosion rate in comparison to values obtained at 0 µm *SiC* grain size. The corrosion rate decreased to 0.386 mm/y and 0.287 mm/y from 1.185 mm/y as earlier mentioned. Further increase in *SiC* grain size to 29 µm and 54 µm did not confer a positive effect on the corrosion rate of AA1070/*SiC* as the corrosion rates increased to 1.479 mm/y and 1.715mm/y, respectively. This observation is probably due to changes in the microstructural and interfacial properties between the enlarged *SiC* grain size and AA1070 matrix. Furthermore, addition of the increased *SiC* grain size could lead to coarse discontinuities in the protective oxide film, thereby causing an increase in number of sites prone to corrosion (Aziz, Qi, & Min, 2009; Trowsdale et al., 1996). This assertion is confirmed from the observation of Brinell hardness values on Table 3 which shows that at 3 µm and 9 µm *SiC* particle size the HV value of AA1070/*SiC* matrix composite increases from 19.6 HV at 0 µm to 35.2 HV and 34.3 HV, respectively. However, increase in the *SiC* particle size to 29 µm and 45 µm caused a significant decrease in Brinell hardness value to 26.2 µm, respectively. The higher HV values obtained at 3 µm and 9 µm *SiC* particle size are due to decrease in porosity within the matrix composite microstructure and hence less discontinuities on the oxide protective film of the composite (Akin et al., 2009; Mashhadi, Khaksaria, & Safi, 2015). Significant cathodic shift was observed on the polarization plots of Figure 1(a) on addition of *SiC* compound (3 µm, 9 µm, 29 µm and 45 µm *SiC* grain sizes) to AA1070 in 0.25M H_2SO_4/0% NaCl due to dominant hydrogen evolution and oxygen reduction reactions on the composite surface. Cathodic polarization is responsible for the destabilization of the oxide film during the activation step, leading to selective dissolution of AA1070/*SiC*. This reaction involves alkalinization of the aluminium/solution boundary during oxygen reduction causing chemical dissolution of the oxide layer (Baeck and Frankel, 2003; Serdechnova, Volovitch, Brisset, & Ogle, 2014).

Table 4. Results of potentiodynamic polarization test for AA1070/*SiC* in 0.25M M H_2SO_4/0%–1% NaCl concentration

0% NaCl								
Sample	***SiC* Grain size (μm)**	**Corrosion rate (mm/y)**	**Corrosion current (A)**	**Corrosion current density (A/cm^2)**	**Corrosion potential (V)**	**Polarization resistance, R_p (Ω)**	**Cathodic Tafel slope, B_c (V/dec)**	**Anodic Tafel slope, B_a (V/dec)**
A	0	1.185	1.09E-04	1.09E-04	−0.581	236.20	−6.739	6.518
B	3	0.386	3.54E-05	3.54E-05	−0.466	725.4	−7.199	5.131
C	9	0.287	2.63E-05	2.63E-05	−0.417	976.00	−6.857	7.365
D	29	1.479	1.36E-04	1.36E-04	−0.420	189.20	−8.595	4.741
E	45	1.715	1.58E-04	1.58E-04	−0.438	138.90	−7.033	4.213
0.25% NaCl								
Sample	***SiC* Grain size (μm)**	**Corrosion rate (mm/y)**	**Corrosion current (A)**	**Corrosion current density (A/cm^2)**	**Corrosion potential (V)**	**Polarization resistance, R_p (Ω)**	**Cathodic Tafel slope, B_c (V/dec)**	**Anodic Tafel slope, B_a (V/dec)**
A	0	1.236	1.14E-04	1.14E-04	−0.519	349.30	−7.847	9.131
B	3	1.033	9.49E-05	9.49E-05	−0.421	268.60	−3.466	18.960
C	9	1.153	1.06E-04	1.06E-04	−0.459	204.10	−9.377	10.380
D	29	2.727	2.51E-04	2.51E-04	−0.476	102.60	−9.484	9.933
E	45	3.178	2.92E-04	2.92E-04	−0.487	62.30	−8.111	8.105
0.5% NaCl								
Sample	***SiC* Grain size (μm)**	**Corrosion rate (mm/y)**	**Corrosion current (A)**	**Corrosion current density (A/cm^2)**	**Corrosion potential (V)**	**Polarization resistance, R_p (Ω)**	**Cathodic Tafel slope, B_c (V/dec)**	**Anodic Tafel slope, B_a (V/dec)**
A	0	1.315	1.21E-04	1.21E-04	−0.489	212.60	−6.180	16.707
B	3	1.143	1.05E-04	1.05E-04	−0.505	223.21	−7.775	22.130
C	9	1.242	1.14E-04	1.14E-04	−0.575	206.70	−7.251	19.450

(*Continued*)

cogent engineering

Table4. (*Continued*)

D	29	1.595	1.47E-04	1.47E-04	−0.577	185.40	−6.068	13.280
E	45	1.687	1.55E-04	1.55E-04	−0.559	142.60	−7.504	13.350
0.75% NaCl								
Sample	***SiC* Grain size (μm)**	**Corrosion rate (mm/y)**	**Corrosion current (A)**	**Corrosion current density (A/cm^2)**	**Corrosion potential (V)**	**Polarization resistance, R_p (Ω)**	**Cathodic Tafel slope, B_c (V/dec)**	**Anodic Tafel slope, B_a (V/dec)**
A	0	2.073	1.90E-04	1.90E-04	−0.533	217.55	−6.099	28.680
B	3	1.797	1.65E-04	1.65E-04	−0.525	261.70	−7.950	22.490
C	9	1.965	1.81E-04	1.81E-04	−0.511	237.21	−7.661	19.100
D	29	2.795	2.57E-04	2.57E-04	−0.541	179.73	−5.309	14.070
E	45	3.065	2.82E-04	2.82E-04	−0.545	125.50	−7.159	17.400
1% NaCl								
Sample	***SiC* Grain size (μm)**	**Corrosion rate (mm/y)**	**Corrosion current (A)**	**Corrosion current density (A/cm^2)**	**Corrosion potential (V)**	**Polarization resistance, R_p (Ω)**	**Cathodic Tafel slope, B_c (V/dec)**	**Anodic Tafel slope, B_a (V/dec)**
A	0	2.251	2.07E-04	2.07E-04	−0.520	124.30	−5.678	22.840
B	3	1.939	1.78E-04	1.78E-04	−0.526	199.55	−8.071	21.33
C	9	2.036	1.87E-04	1.87E-04	−0.505	234.84	−7.301	18.396
D	29	2.919	2.68E-04	2.68E-04	−0.493	96.20	−7.540	19.111
E	45	3.261	3.00E-04	3.00E-04	−0.509	78.80	−7.343	15.310

cogent engineering

At 0.25%–1% NaCl concentration, the corrosion rates of AA1070/*SiC* at 3 μm and 9 μm *SiC* grain sizes are marginally lower than the corrosion rate of AA1070/*SiC* at 0 μm *SiC* grain size; however, a proportionate increase in value at these *SiC* grain sizes (3 μm and 9 μm) was observed with increase in NaCl concentration. As earlier observed, AA1070/*SiC* at 29 μm and 45 μm *SiC* grain size significantly reduced the corrosion resistance of AA1070/*SiC* in 0.25 M H_2SO_4/0.25%–1% NaCl. Their corrosion rates were observed to increase with increase in NaCl concentration. Cathodic shift also occurred on the polarization plots of AA1070/*SiC* [Figure 1(b)] at 3 μm, 29 μm and 45 μm in 0.25 M H_2SO_4/0.25% NaCl solution for reasons earlier discussed; however, from 0.25 M H_2SO_4/0.5%–1% NaCl minimal anodic shift was observed on the polarization plots [Figure 1(c)–(e)] due to increase in dissolution rate of AA1070/*SiC* resulting from increased Cl^- ion concentration. This phenomenon results in extensive localized attack of Cl^- ions and is attributed to galvanic action between the enlarged *SiC* grains (Loto & Adeleke, 2016; Reena, Nayak, & Nityanand, 2016). The corrosion resistance characteristic of AA1070/*SiC* is associated closely with its *SiC* grain size, which might be responsible for the limited formation of second-phase precipitates and interaction products. Optical microscopy analysis of AA1070/*SiC* morphology (to be discussed later) shows the presence corrosion pits formed on AA1070/*SiC* than in AA1070 alloy.

3.2. Open circuit potential (OCP) measurement

The thermodynamic stability of AA1070/*SiC* at 0 μm, 3μm, 9 μm, 29 μm and 45 μm *SiC* grain sizes in 0.25 M H_2SO_4/0%, 0.25% and 1% NaCl are shown in the graphical plots of OCP versus exposure time [Figure 2(a)–(c)]. OCP values for AA1070/*SiC* at 0 μm *SiC* in 0.25 M H_2SO_4/0% NaCl [Figure 2(a)] tend to be more electronegative than AA1070/*SiC* at higher *SiC* grain sizes, thus more likely to participate in the electrochemical corrosion reactions in the acid chloride solution without applied potential (Hoar, 1967; Hoar & Jacob, 1967). At 0s, its OCP value (−0.505 mV) decreased to −0.565 mV at 127s due to active electrochemical reactions, before increasing progressively to −0.479 mV at 1,500 s. Similar OCP behaviour was observed for AA1070/*SiC* at 3 μm *SiC*, but at higher OCP values. The OCP values for AA1070/*SiC* at 9 μm, 29 μm and 45 μm *SiC* grain sizes showed relative thermodynamic stability at much higher potentials.

Addition of 0.25% NaCl [Figure 2(b)] to the electrolyte solution did not necessarily change the dynamics of the OCP curves compared to Figure 2(a); however, potential transients are visible due to current flow from localized corrosion sites on AA1070/*SiC* as a result of the presence of Cl^- ions (Strehblow, 1984). The potential transients are absent on AA1070/*SiC* (0 μm *SiC*) between potentials of −0.555V and −0.529V despite visible change in the OCP curve probably due to electrochemical dynamics associated with repassivation of the oxide layer on the composite (Stellwag, 1998). Potential transients were completely absent from AA1070/*SiC* (3 μm *SiC*) despite relative thermodynamic instability throughout the exposure hours due to higher resistance of AA1070/*SiC*

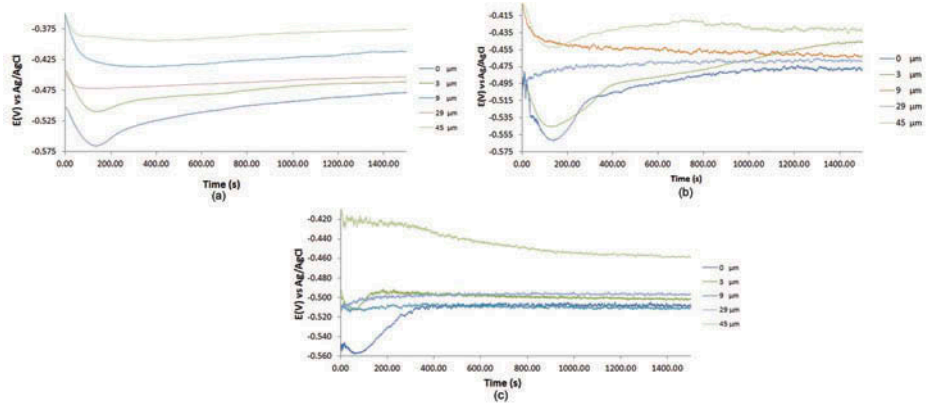

Figure 2. Plot of corrosion potential versus exposure time for AA1070/*SiC* in (a) 0.25 M H_2SO_4/0% NaCl, (b) 0.25 M H_2SO_4/0.25% NaCl and (c) 0.25 M H_2SO_4/0.25% NaCl.

at 3 μm grain size. This observation agrees with the result from the polarization test. At higher *SiC* grain size, the OCP values shift to noble potentials, indicating higher thermodynamic stability as earlier mentioned. At 1% NaCl [Figure 2(c)], the effect of *SiC* grain size seems too negligible with respect to thermodynamic stability of AA1070/*SiC* within the electrolyte with minimal variation between −0.509V (0 μm) and −0.497V (29 μm) at 1,500 s; however, at 45 μm there is a large anodic shift to −0.401V (0s) and −0.459V (1500s). Potential transients are clearly visible through the exposure hours at all *SiC* grain sizes due to excess Cl^- ions. Delineation of the results from OCP shows addition of *SiC* of different grain size shifts the overall OCP plots of AA1070/*SiC* anodically. Though it does not necessarily improve the corrosion resistance, it actually improves the thermodynamic stability of the composite in the acid chloride media.

3.3. Optical microscopy analysis

Optical microscopic images of AA1070 and AA1070/*SiC* surface morphologies before and after corrosion at magnification ×40 are shown from Figures 3 to 6(e). Figure 3 shows the general morphology of AA1070 and AA1070/*SiC* before corrosion test. The morphologies of AA1070 and AA1070/*SiC* after corrosion in 0.25 M H_2SO_4/0% NaCl media [Figure 4(a)–(e)] are quite similar to the morphology in Figure 3. There seems to be no significant alteration on the surface features of the aluminium composite in the presence of SO_4^{2-} ions in the acid media with respect to *SiC* grain size except for mild deterioration due to wear, resulting from charge transfer reaction of the SO_4^{2-} ions. This shows the composite is reasonably resistant to corrosion in the absence of Cl^- ions. Images [Figure 5(a)–4(e)] from 0.25 M H_2SO_4/0.25% NaCl media showed a marked difference from their counterparts in Figure 4(a)–(e). The presence of corrosion pits is quite visible with respect to *SiC* grain size. AA1070 at 0 μm grain size [Figure 5(a)] showed the highest pitting corrosion resistance whereby its morphological deterioration tends to be shallow compared to AA1070/*SiC* at 3 μm, 9 μm, 29 μm and 45 μm [Figure 5(b)–(e)]. Second, higher *SiC* grain size connotes more and deeper micropits on the composite surfaces. Formation of corrosion pits occurs due to adsorption of Cl^-ions at discontinuities in the surface oxide film resulting from chemical reaction between the Cl^- ions and valence electrons on the aluminium matrix (Foley, 1986). The nonhomogeneous properties of the composite most importantly involving the reaction of *SiC* and the aluminium matrix dominate the outcome reaction of the composite with its environment (Nunes & Ramanathan, 1995). The visible corrosion features on AA1070/*SiC* morphology corrosion than AA1070 are due to galvanic action due to lack of continuous surface oxide on the composite (Reena et al., 2016). Microstructural anomalies and processing factors also play a major role because at 29 μm *SiC* grain size the depth of AA1070/*SiC* pitted surface seems more shallow than at 9 μm *SiC* grain size (Gnecco & Beccaria, 1999; Hihara, 2005; Trzaskoma, 1990). Figure 6(a)–(e) shows the morphology of AA1070/*SiC* of different grain size from 0.25 M H2SO4/1% NaCl solution. Severe

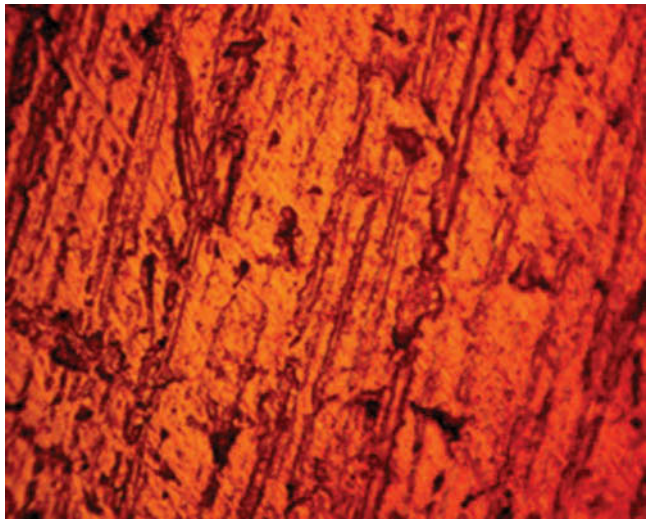

Figure 3. Optical image of AA1070 before corrosion.

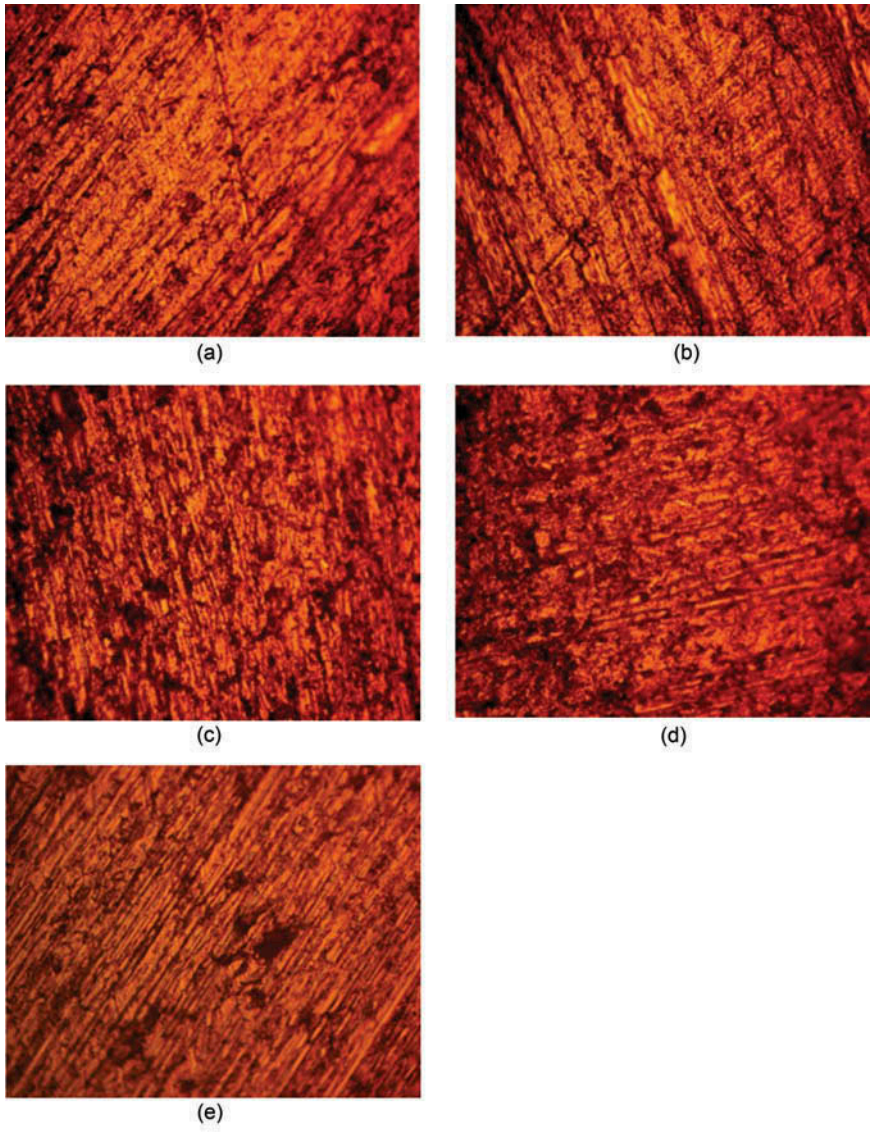

Figure 4. Optical images of AA1070/*SiC* at magnification ×40 after corrosion in 0.25 M H_2SO_4/0% NaCl (a) 0 µm *SiC* grain size, (b) 3 µm *SiC* grain size, (c) 9 µm *SiC* grain size, (c) 29 µm *SiC* grain size and (d) 45 µm *SiC* grain size.

deterioration can be observed with respect to *SiC* content; however, the extent of deterioration is much more severe for AA1070/*SiC* at 29 µm and 45 µm *SiC* grain size [Figure 6(d), (e)] with deep corrosion pits prevalent in Figure 6(e).

3.4. Statistical analysis

Table 5 shows ANOVA results on the statistical importance of *SiC* grain size variation and NaCl concentration on the corrosion resistance of AA1070/*SiC*. Both *SiC* grain size and NaCl concentration prove to be statistically relevant with *F* values of 14.92 and 8.76. The values are most importantly greater than the theoretical significance factor (significance *F*) of 3.86. The *F* values correspond to a percentage significance of 55.9% for *SiC* grain size and 32.8 for NaCl concentration. Despite the significant effect of NaCl concentration on AA1070/*SiC* corrosion, statistical results show that variation in *SiC* grain size has stronger influence on the corrosion resistance of AA1070/*SiC* matrix composite. Result from potentiodynamic polarization shows that *SiC* grain size at 3 µm and 9 µm gave the lowest corrosion rate values; hence limiting the *SiC* particle size in matrix

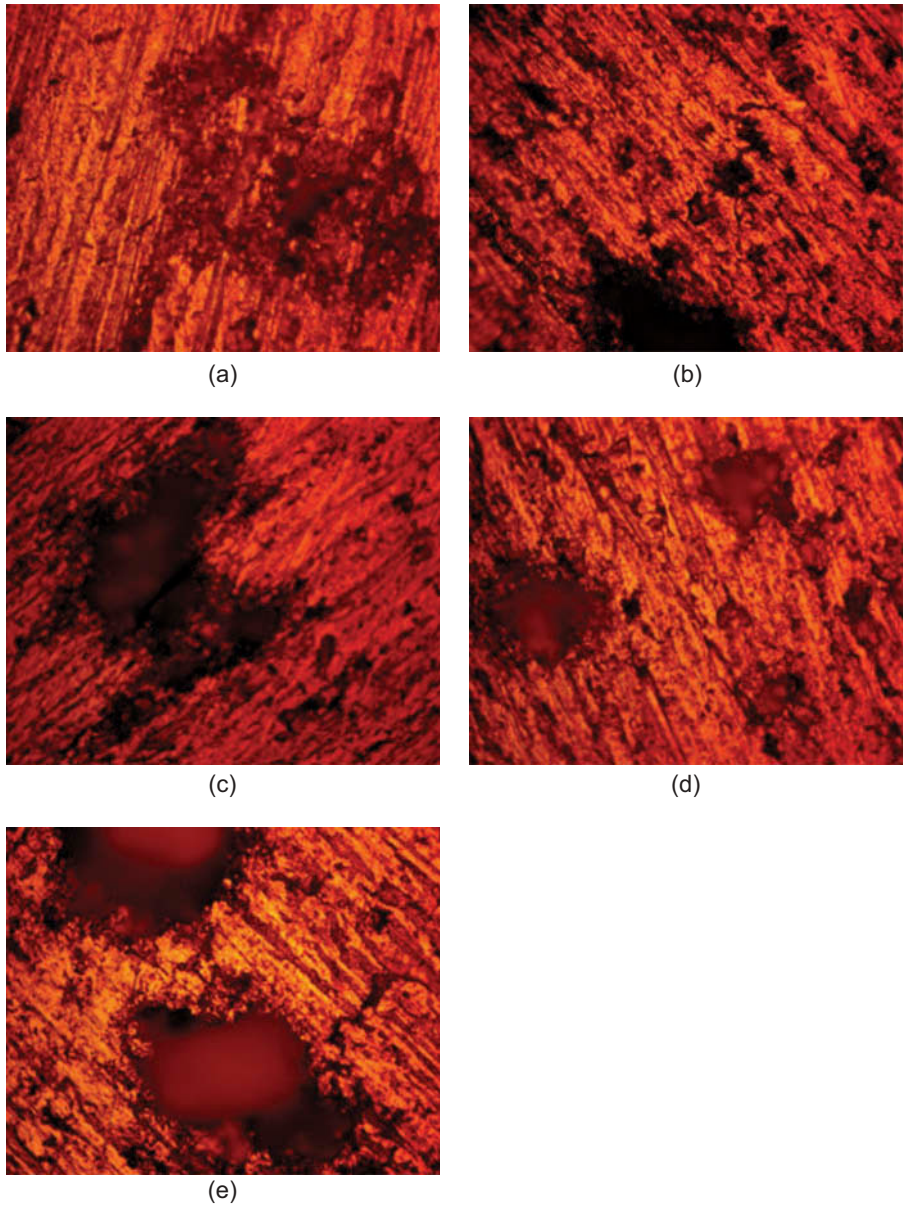

Figure 5. Optical images of AA1070/*SiC* at magnification ×40 after corrosion in 0.25 M H_2SO_4/0.25% NaCl (a) 0 µm *SiC* grain size, (b) 3 µm *SiC* grain size, (c) 9 µm *SiC* grain size, (c) 29 µm *SiC* grain size and (d) 45 µm *SiC* grain size.

composites improves the corrosion resistance properties of the matrix composite in chloride-containing environments.

4. Conclusion

SiC grain size variations significantly influence the corrosion resistance properties and OCP values of AA1070 aluminium matrix composite in acid chloride media. Low *SiC* grain size had a positive effect on the matrix alloy, while higher *SiC* grain size increased the corrosion resistance susceptibility of the aluminium matrix due to galvanic action among the intermetallic precipitates. Cathodic corrosion potential shift at low *SiC* grain size is due to cathodic polarization of the matrix surface, while the anodic shift at higher *SiC* grain size is due to anodic deterioration of the matrix alloy. *SiC* grain size tends to be more statistically relevant on the matrix alloy corrosion resistance from ANOVA analysis. Microanalytical studies show pitted morphology of the aluminium matrix for

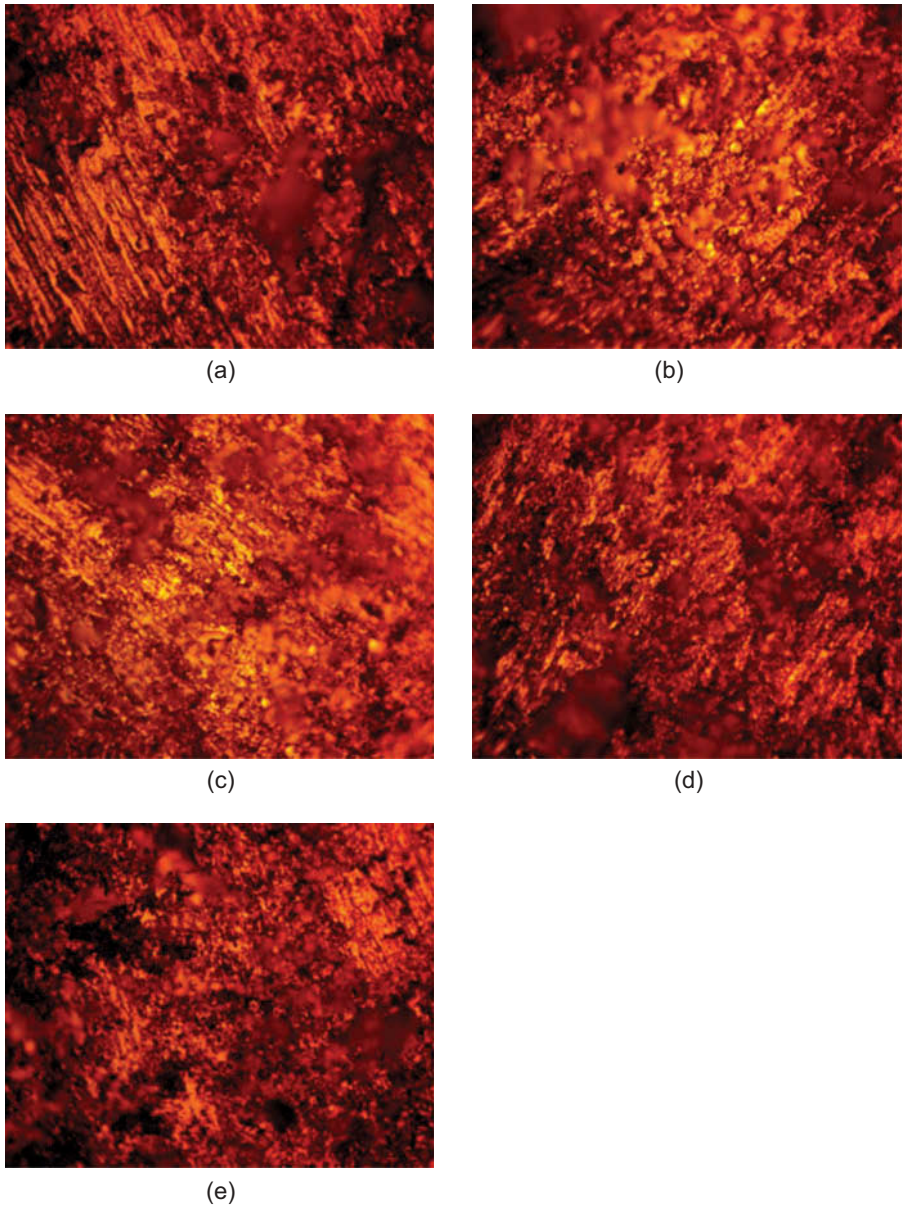

Figure 6. Optical images of AA1070/*SiC* at magnification ×40 after corrosion in 0.25 M H_2SO_4/1% NaCl (a) 0 µm *SiC* grain size, (b) 3 µm *SiC* grain size, (c) 9 µm *SiC* grain size, (c) 29 µm *SiC* grain size and (d) 45 µm *SiC* grain size.

Table 5. Data on the statistical importance of *SiC* grain size and NaCl concentration on AA1070/*SiC* corrosion in 0.25 M H_2SO_4/(0%–1% NaCl) at 95% confidence level

Source of variation	Sum of squares	Degree of freedom	Mean square	Mean square ratio (*F*)	Significance *F*	*F* (%)
NaCl concentration	3.03	3	1.01	8.76	3.86	32.8
SiC grain size	5.17	3	1.72	14.92	3.86	55.9
Residual	1.04	9	0.12			
Total	9.24	15				

all *SiC* grain size at low chloride concentration, while the morphology of the aluminium matrix at higher chloride concentration showed total degradation.

Acknowledgements
The authors acknowledge Covenant University Ota, Ogun State, Nigeria, for the sponsorship and provision of research facilities for this project.

Funding
This work was supported by the Covenant University.

Author details
Roland Tolulope Loto[1]
E-mail: tolu.loto@gmail.com
Phillip Babalola[1]
E-mail: phillip.babalola@covenantuniversity.edu.ng
[1] Department of Mechanical Engineering, Covenant University, Ota, Nigeria.

Citation information
Cite this article as: Analysis of *SiC* grain size variation and NaCl concentration on the corrosion susceptibility of AA1070 aluminium matrix composites, Roland Tolulope Loto & Phillip Babalola, *Cogent Engineering* (2018), 5: 1473002.

References

Akin, I., Hotta, M., Sahin, F. C., Yucel, O., Goller, G., & Goto, T. (2009). Microstructure and densification of ZrB_2–SiC composites prepared by spark plasma sintering. *Journal of the European Ceramic Society*, *29*(11), 2379–2385. doi:10.1016/j.jeurceramsoc.2009.01.011

Aziz, I., Qi, Z., & Min, X. (2009). Corrosion inhibition of SiCp/5A06 aluminum metal matrix composite by cerium conversion treatment. *Chinese Journal Aeronautics*, *22*(6), 670–676. doi:10.1016/S1000-9361(08)60157-0

Baeck, Y., & Frankel, G. S. (2003). Electrochemical quartz crystal microbalance study of corrosion of phases in AA 2024. *Journal of Electrochemical Society*, *150*(1), B1–B9. doi:10.1149/1.1524172

Bakkar, A., & Neubert, V. (2007). Corrosion characterization of alumina–Magnesium metal matrix composites. *Corrosion Science*, *49*(3), 1110–1130. doi:10.1016/j.corsci.2006.07.002

Candan, S., & Biligic, E. (2004). Corrosion behavior of Al–60 vol.% SiCp composites in NaCl solution. *Materials Letters*, *58*(22–23), 2787–2790. doi:10.1016/j.matlet.2004.04.009

Chawla, K. K. (2013). *Composite materials: Science and engineering*. New York, NY: Springer-Verlag. doi:10.1007/978-0-387-74365-3

Foley, R. T. (1986). Localized corrosion of aluminum alloys —A review. *Corrosion*, *42*(5), 277–288. doi:10.5006/1.3584905

George, E., Totten, D., & Scott, M. (2003). *Handbook of aluminum alloy production and materials manufacturing* (Vol. 2). New York, NY: Taylor & Francis Inc.

Gnecco, F., & Beccaria, A. M. (1999). Corrosion behaviour of Al–Si/SiC composite in sea water. *British Corrosion Journal*, *34*(1), 57–62. doi:10.1179/bcj.1999.34.1.57

Griffiths, A. J., & Turnbull, A. (1994). An investigation of the electrochemical polarization behaviour of 6061 aluminum metal matrix composites. *Corrosion Science*, *36*(1), 23–35. doi:10.1016/0010-938X(94)90106-6

Hashim, J., Looney, L., & Hashmi, M. S. J. (2002). Particle distribution in metal matrix composites, part-I. *Journal of Materials Processing Technology*, *123*(2), 251–257. doi:10.1016/S0924-0136(02)00098-5

Hihara, L. H. (2005). Corrosion of metal-matrix composites. *ASM Handbook*, *13B*, 526–542.

Hoar, T. P. (1967). The production and breakdown of the passivity of metals. *Corrosion Science*, *7*(6), 341–355. doi:10.1016/S0010-938X(67)80023-4

Hoar, T. P., & Jacob, W. R. (1967). Breakdown of passivity of stainless steel by halide ions. *Nature*, *216*, 1299–1301. doi:10.1038/2161299a0

Lees, J. K., Dhihra, A. K., & McCullough, R. L. (2005). *Composite materials*. Wiley-VCH Verlag GmbH & Co.

Loto, R. T., & Adeleke, A. (2016). Corrosion of aluminum alloy metal matrix composites in neutral chloride solutions. *Journal of Failure Analysis and Prevention.*, *16*(5), 874–885. doi:10.1007/s11668-016-0157-3

Loto, R. T., & Babalola, P. (2017). Corrosion polarization behavior and microstructural analysis of AA1070 aluminium silicon carbide matrix composites in acid chloride concentrations. *Cogent Engineering*, *4*, 1. doi:10.1080/23311916.2017.1422229

Mahendra, B. M., Arulshri, K., & Iyandurai, N. (2013). Evaluation of mechanical properties of aluminium alloy 2024 reinforced with silicon carbide and fly ash hybrid metal matrix composites. *American Journal of Applied Science*, *10*(3), 219–229. doi:10.3844/ajassp.2013.219.229

Mashhadi, M., Khaksaria, H., & Safi, S. (2015). Pressureless sintering behavior and mechanical properties of ZrB_2–SiC composites: Effect of SiC content and particle size. *Journal of Materials Research and Technology*, *4*(4), 416–422. doi:10.1016/j.jmrt.2015.02.004

Neelima, D. C., Mahesh, V., & Selvaraj, N. (2011). Mechanical characterization of aluminium silicon carbide composite. *International Journal of Applied Engineering Research*, *1*(4), 793–799.

Nunes, P. C. R., & Ramanathan, L. V. (1995). Corrosion behavior of alumina-aluminum and silicon carbide-aluminum metal-matrix composites. *Corrosion*, *51*(8), 610–617. doi:10.5006/1.3293621

Pai, B., Rajan, T., & Pillai, R. (2004). Aluminium matrix composite castings for automotive applications. *Indian Foundry*, *50*(9), 30–39.

Reena, K. P. D., Nayak, J., & Nityanand, S. A. (2016). Corrosion behavior of 6061/Al-15 vol. pct. SiC(p) composite and the base alloy in sodium hydroxide solution. *Arabian Journal of Chemistry*, *9*(2), S1144–S1154. doi:10.1016/j.arabjc.2011.12.003

Serdechnova, M., Volovitch, P., Brisset, F., & Ogle, K. (2014). On the cathodic dissolution of Al and Al alloys. *Electrochimica Acta*, *124*(2014), 9–16. doi:10.1016/j.electacta.2013.09.145

Sinclair, I., & Gregson, P. J. (1997). Structural performance of discontinuous metal matrix composites. *Materials Science and Technology*, *13*(9), 709–726. doi:10.1179/mst.1997.13.9.709

Singh, R., & Singla, E. (2012). Tribological characterization of aluminium-silicon carbide composite prepared by mechanical alloying. *International Journal of Applied Engineering Research*, *7*(11), 1420–1423.

Singla, M., Dwivedi, D., Singh, L., & Chawla, V. (2009). Development of aluminium based silicon carbide particulate metal matrix composite. *Journal of Minerals & Materials Characterization & Engineering*, *8*(6), 455–467. doi:10.4236/jmmce.2009.86040

Stellwag, B. (1998). The mechanism of oxide film formation on austenitic stainless steels in high temperature water. *Corrosion Science*, *40*(2–3), 337–370. doi:10.1016/S0010-938X(97)00140-6

Strehblow, H. H. (1984). Breakdown of passivity and localized corrosion: Theoretical concepts and fundamental experimental results. *Materials and Corrosion*, *35*(10), 437–448. doi:10.1002/maco.19840351002

Surappa, M. K. (2003). Aluminium matrix composites: Challenges and opportunities. *Sadhana*, *28*(1–2), 319–334. doi:10.1007/BF02717141

Trowsdale, A. J., Noble, B., Harris, S. J., Gibbins, I. S. R., Thompson, G. E., & Wood, G. C. (1996). The influence of silicon carbide reinforcement on the pitting behaviour of aluminium. *Corrosion Science*, *38*(2), 177–191. doi:10.1016/0010-938X(96)00098-4

Trzaskoma, P. P. (1990). Pit morphology of aluminum alloy and silicon carbide/aluminum alloy metal matrix composites. *Corrosion*, *46*(5), 402–409. doi:10.5006/1.3585124

William, D. C., Jr. (2007). *Materials science and engineering an introduction* (7th ed.). New York, NY: Wiley.

Cogent Engineering **(ISSN: 2331-1916) is published by Cogent OA, part of Taylor & Francis Group.**

Publishing with Cogent OA ensures:

- Immediate, universal access to your article on publication
- High visibility and discoverability via the Cogent OA website as well as Taylor & Francis Online
- Download and citation statistics for your article
- Rapid online publication
- Input from, and dialog with, expert editors and editorial boards
- Retention of full copyright of your article
- Guaranteed legacy preservation of your article
- Discounts and waivers for authors in developing regions

Submit your manuscript to a Cogent OA journal at www.CogentOA.com